Sensors and Materials, Vol. 37, No. 12 (2025) 5625–5636
MYU Tokyo

S & M 4268

Pressure Analyses of Instant Turbulence and Vibration between Two Passing High-speed Trains

Yan-Zuo Chang,[1] Yan-Cheng Cao,[2] Bo-Wun Huang,[2]
Chao-Ming Hsu,[2*] and Cheng-Fu Yang[3,4**]

[1]School of Technology, Fuzhou Technology and Business University, Fuzhou, Fuian 350715, China
[2]Department of Mechanical Engineering, National Kaohsiung University of Science and Technology, Kaohsiung 807, Taiwan
[3]Department of Chemical and Materials Engineering, National University of Kaohsiung, Kaohsiung 811, Taiwan
[4]Department of Aeronautical Engineering, Chaoyang University of Technology, Taichung 413, Taiwan

(Received June 5, 2025; accepted November 28, 2025)

Keywords: Ansys Fluent, instant turbulence, vibration analysis, high-speed train

In this study, we aimed to mitigate the turbulence and vibration effects encountered when two high-speed trains pass each other by employing the software Ansys Fluent for simulations. By comparing the simulation results with existing literature on the interaction of high-speed trains passing alongside each other in various environments, we evaluated whether the established simulation model accurately reflects real-world pressure curves measured by sensors during the passing moment. To minimize the turbulent effects while the trains are in motion, we investigated the feasibility of installing stabilizing flow wings on the exterior of the front end of the trains. The objective was to determine whether these modifications could effectively reduce turbulence and improve train stability. The research included simulations where different configurations of stabilizing flow wings were tested, such as various widths, lengths, quantities, and positions of the wings. These different designs were simulated to evaluate their impact on reducing turbulence during train interactions. The findings suggest that adding stabilizing flow wings to the front ends of the trains can reduce the turbulence-induced effects by approximately 37% when two high-speed trains pass each other. This reduction in turbulence can lead to improved safety, comfort, and operational efficiency for high-speed rail systems, particularly in environments where high-speed trains frequently encounter each other.

1. Introduction

As high-speed rail networks continue to expand globally, the aerodynamic interactions between passing trains at elevated velocities present increasing challenges for both passenger comfort and operational safety. In recent years, countries have continuously pushed the limits of the maximum operating speeds of high-speed trains. As these speed limits are being continually broken, various issues related to air resistance and its impact on train performance have emerged. In addition to the challenge of overcoming air resistance at high speeds, the stability of

*Corresponding author: e-mail: jammy@nkust.edu.tw
**Corresponding author: e-mail: cfyang@nuk.edu.tw
https://doi.org/10.18494/SAM5795

ISSN 0914-4935
https://myukk.org/

the train while traveling at high velocity has become increasingly important. Apart from the air resistance faced by a train during individual high-speed, straight-line travel, the pressure differences and turbulence effects created at the moment of train interactions are also critical factors influencing the stability of high-speed trains. These lateral pressure changes significantly affect the train's performance. If the pressure difference becomes too great, it can lead to vibrations that damage the train's structure, cause discomfort to passengers, and, in the worst-case scenario, could even result in a derailment due to the sudden pressure discrepancy during the event, potentially leading to severe accidents.

Niu *et al.* investigated the impact of train length on air pressure fluctuations when high-speed trains pass each other in tunnels.(1) They modeled full-scale trains of different lengths traveling through tunnels and employed a sliding mesh technique in their finite element simulations. The validity of their simulation framework was demonstrated through comparison with pressure sensor measurements obtained from actual trains. Their results confirmed that the sliding mesh approach can reliably reproduce the aerodynamic behavior of high-speed train operations, and their analysis of the pressure distribution along the train bodies successfully identified regions subjected to higher aerodynamic loading. These findings enable the enhancement of structural safety in train design. Additional study revealed that different tunnel designs significantly influence air pressure effects on high-speed trains.(2) Deng *et al.* examined the aerodynamic loads and corresponding aerodynamic phenomena affecting high-speed trains passing alongside windbreak walls and through windbreak tunnels under crosswind conditions.(3) Their methodology combined actual pressure sensor data from high-speed trains with computer simulations to develop models for windbreak walls and tunnels. Simulation results were validated by comparing them with pressure sensor measurements. Windbreak tunnels were found to perform more effectively in areas with significant crosswind influence, and the substantial impact of crosswinds on high-speed train operations was confirmed.(4,5)

The above literature indicated that a suitable design of the front end of high-speed trains can significantly enhance stability and reduce drag and pressure effects at high speeds. Additionally, the Reynolds number can influence the simulation.(6) Within an appropriate range of Reynolds numbers and with proper grid planning, the simulation results can closely match actual measurement results. Crosswinds can have a considerable impact on the train, while the design and optimization of the bogie also affect the airflow beneath the train. Materials under pressure on the tracks can alter the airflow under the vehicle as well. Installing deflectors on the exterior of high-speed trains can affect pressure changes on the train's surface. Tunnel design is also crucial for the movement of high-speed trains, as it can impact the train's airflow. The pressure changes that occur when two high-speed trains pass each other in a tunnel are much greater than when a single train passes through. Therefore, simulation results should be compared with actual pressure changes observed during high-speed train operation to ensure accurate simulations.

Proper calibration between simulated and actual pressure variations is essential for enhancing the precision of predictive models, contributing to better engineering outcomes and safer high-speed rail systems. The air resistance and pressure encountered by high-speed trains during operation are closely linked to overall aerodynamic performance, and reducing these forces is critical for maintaining stability during high-speed train travel. Minimizing both air resistance

and pressure not only improves operational stability but also reduces the aerodynamic drag experienced by the train. Furthermore, an optimized aerodynamic shape enhances energy efficiency by enabling smoother airflow around the vehicle. In this study, we focused specifically on the critical moment when two high-speed trains pass each other, during which large transient pressure changes and intense turbulence are generated.

To clearly address the design modification explored in this work, we provide a detailed description of the structural changes implemented on the trains. In addition to clarifying the design modifications investigated, it is also important to highlight what distinguishes the present simulation from previously published studies. First, the computational model in this work was constructed using the full three-dimensional dimensions of an actual high-speed train, resulting in a train length of 90 m, width of 1.8 m, and height of 3.8 m. Most earlier aerodynamic studies adopted simplified, shortened, or scaled-down geometries to reduce computational cost, whereas the use of true full-scale dimensions in our model enables a more realistic representation of the surrounding flow field during high-speed operation. Because the train dimensions were modeled at full scale, the airflow domain required for the finite element simulation was also significantly expanded to prevent artificial boundary effects and to ensure accurate development of the turbulent structures prior to the train-passing event.

Second, the novelty of this study lies in proposing and systematically evaluating the configuration of a stabilizer wing mounted on the exterior sides of the train nose, a design concept that, to our knowledge, has not been examined in the context of two-train-passing aerodynamics. To determine whether such structural additions can effectively suppress the severe turbulence generated during high-speed encounters, we conducted detailed parametric simulations involving different stabilizer-wing positions, various numbers of stabilizer wings, and multiple geometric dimensions of, for example, the wing length and width. By combining a full-scale three-dimensional train model with a novel stabilizer-wing aerodynamic modification, we provide a simulation framework that differs substantially from those in previously published works. The resulting analysis offers new insight into how targeted geometric alterations can mitigate pressure effects during high-speed train passing, thereby improving train stability and enhancing operational safety.

2. Simulation Parameters

In the current study, we employed Ansys Fluent computational fluid dynamics software to simulate the transient aerodynamic interactions during high-speed train passing events. Our model incorporates detailed train geometries, realistic operational parameters, and environmental conditions to ensure simulation accuracy. The computational domain was carefully designed with appropriate mesh refinement in critical regions to capture the rapid pressure fluctuations and complex vortex structures that develop during train passing. In this study, we conducted computer simulation analysis using the commercial software Solidworks. We also referenced the designs of high-speed trains from various countries and created simple models of two high-speed trains using the actual sizes, as shown in Fig. 1(a). Because of the simplicity of the model, the train's bogies, wheels, and tracks were not considered in this study.

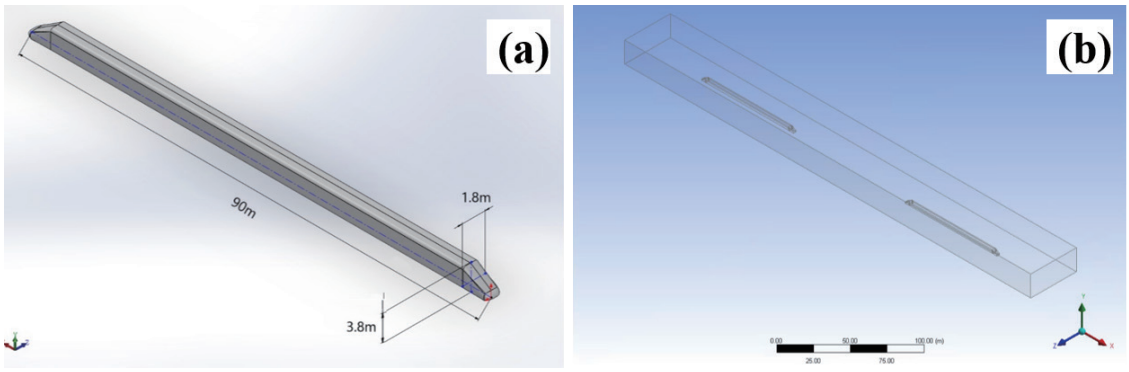

Fig. 1. (Color online) Illustrations of (a) the dimensions (length, width, and height) of a single high-speed train and (b) the aerodynamic flow field around a high-speed train.

Once the physical model was established, the next step involved the use of the commercial finite element software Ansys Workbench for meshing and element selection to create the finite element model. The flow field was then simulated using the Fluent module within Ansys Workbench. The simulation results obtained were compared with data from other literature to confirm that the simulation model aligns with real-world conditions.

The model was established using the real three-dimensional dimensions of a high-speed train, including its length, width, and height. The length of a single high-speed train is 90 meters, the width is 1.8 m, and the height is 3.8 m. For simplicity, the train body was modeled without including the bogie and wheels. The lateral spacing between two trains was 4.6 meters, and the height of the train bottom from the ground was 0.2 meters. The relative distance between the two trains was set at 100 meters. By increasing the relative distance between the two high-speed trains in the simulation, a more stable pressure variation around the trains could be achieved before simulating the process of two trains passing each other. The air flow field for the finite element simulation was developed using research data from the literature. Since the dimensions of the high-speed train in the model correspond to real-world train measurements, the surrounding air flow field also needed to be quite large. As shown in Fig. 1(b), this ensured that the simulation accurately reflects the real-world conditions for aerodynamic analysis and pressure variations.

In this simulation, we utilized a three-dimensional model based on actual high-speed train dimensions. Given the complex curved surfaces of the train model and the need for numerous mesh elements to achieve more precise solution data, tetrahedral meshes were employed for the train's grid planning. These meshes were categorized into small-size (0–100 mm), medium-size (500–1000 mm), and large-size (500–1000 mm) grids. The mesh size progressively increases from the train nose to the train head and then to the train body, as illustrated in Fig. 2(a), with the post-partitioning mesh distribution shown in Fig. 2(b). Because of the high mesh count in this simulation and in order to optimize the computational time and data volume, mesh refinement was selectively applied only to regions significantly impacting the solution data, while larger mesh elements were utilized for the remaining portions.

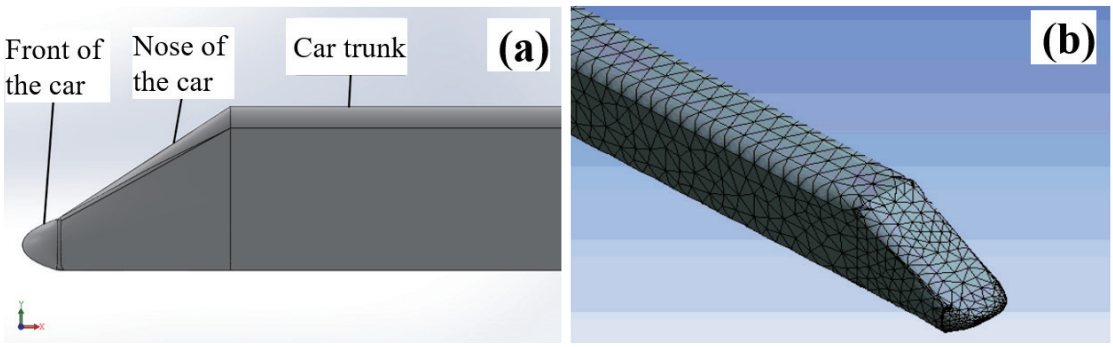

Fig. 2. (Color online) (a) Schematic diagram of the train components and (b) mesh diagram of the high-speed train.

3. Simulation Results and Discussion

The wind pressure and turbulence results generated at the moment of high-speed train passings constitute key data in this study. Because the model is fully three-dimensional, the selection of pressure and turbulence evaluation regions within the simulation is critical. The aerodynamic loads experienced at different positions on the train surface vary considerably, and thus carefully defining these evaluation locations is essential for accurately capturing the spatial characteristics of the pressure and turbulence fields. Each part of the train, from the nose, front, body, to the tail, experiences different impacts during the high-speed train passing, as shown in Fig. 3. In Fig. 3, the color distribution represents the pressure distribution. As shown in Fig. 3(d), blue indicates the minimum pressure and red indicates the maximum pressure, while the gradual color transitions correspond to changes in pressure. The positioning of the measurement points, as discussed in the papers by Muñoz-Paniagua and García[7] and Bell *et al.*,[8] reveals that different parts of a high-speed train experience varying impacts when traveling at high speeds. Specifically, the nose and the sides of the front of the train typically show larger pressure variations. According to their studies, the areas with the most significant variations are generally located in the lower half of the train body. When two high-speed trains pass each other at high speed, the nose and the sides of the front will experience substantial pressure changes, with the largest changes usually occurring in the lower half of the train body. Furthermore, the side of the train's front is where turbulence tends to be most intense. Considering all these factors, it becomes clear that the area with the most significant turbulence generation is the lower half of the side of the front of the train, as Fig. 3(d) shows.

As demonstrated in the paper by Muñoz-Paniagua and García,[7] this observation holds true. Additionally, the greatest pressure difference during the moment of the high-speed train passing occurs between the fronts of the two trains. Therefore, we focus on the lower half of the front-to-front region between the two trains as the primary pressure evaluation area, as illustrated in Figs. 3(b) and 3(c). Because the maximum negative pressure and the most intense turbulence are typically generated near the central region where the two train noses align, the simulation primarily concentrates on this central passing zone when determining the pressure evaluation positions. This approach underscores the importance of appropriately selecting simulation

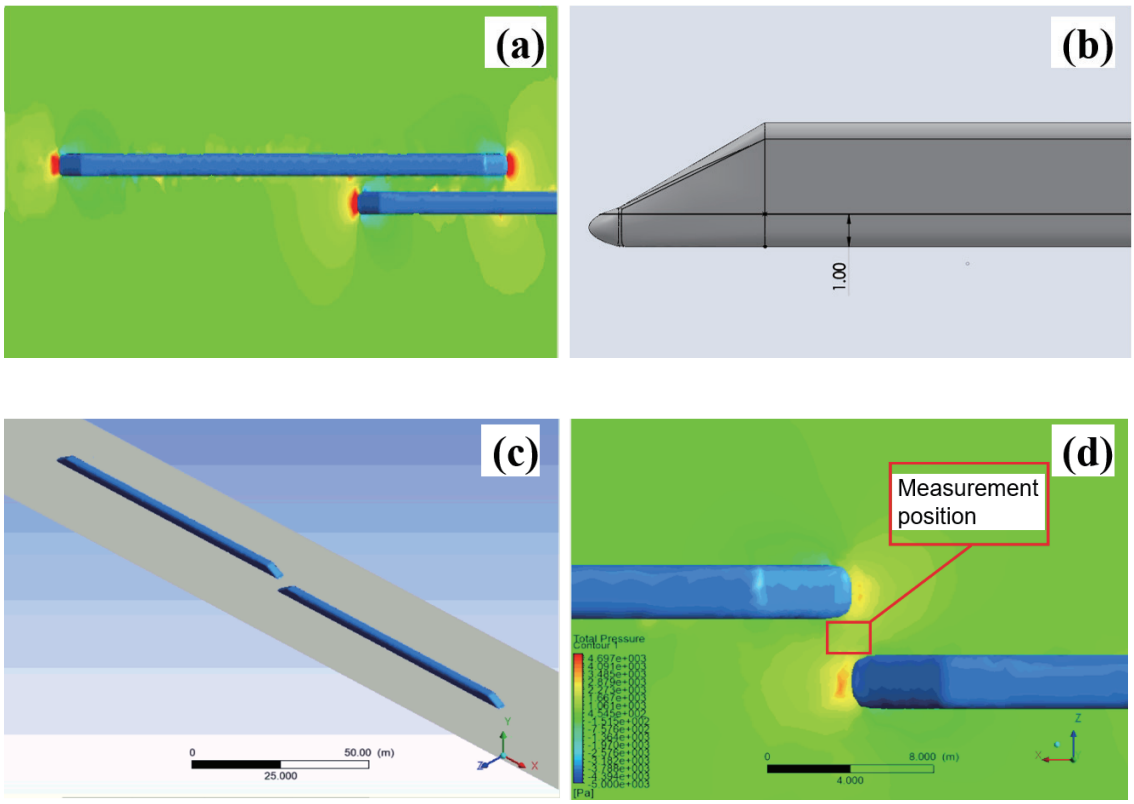

Fig. 3. (Color online) (a) Pressure distribution diagram of the high-speed train, (b) height position diagram for contour extraction from simulation results, (c) range diagram for contour extraction from simulation results, and (d) schematic diagram of simulation-based pressure evaluation locations.

evaluation regions to accurately capture the dynamic aerodynamic effects that occur during high-speed train passings. The results suggest that the lower half of the front sides of the train are particularly sensitive to pressure and turbulence variations. These insights are crucial for designing trains that can better withstand aerodynamic forces during high-speed travel. Furthermore, understanding the behavior of turbulence and pressure in these critical areas can help in optimizing train shape, improving stability, and ensuring passenger comfort.

In this study, we aimed to validate the simulation results using the experimental data of pressure sensing effects found in both domestic and international research papers and journals. By referencing the works of scholars such as Huang *et al.*[9] and Gao *et al.*,[10] we used the experimental parameters and data from their papers to simulate and analyze the interactions between high-speed trains during a passing event. The finite element analysis (FEA) simulation results were then organized and plotted with the raw data. Upon comparing the experimental results from the referenced papers with the FEA simulation data, we observed that with each train traveling at a speed of 430 km/h, the pressure at the simulation-based pressure evaluation locations on the train bodies gradually increased as the train fronts begin to pass each other at 2.9 s (not shown here). At 3.0 s, the maximum positive pressure occurred, as shown in Fig. 4(a). Subsequently, the pressure dropped sharply to a negative pressure at 3.05 s, as shown in Fig. 4(b). At 3.1 s (not shown here) and 3.15 s, as the peak negative pressure area has passed, the

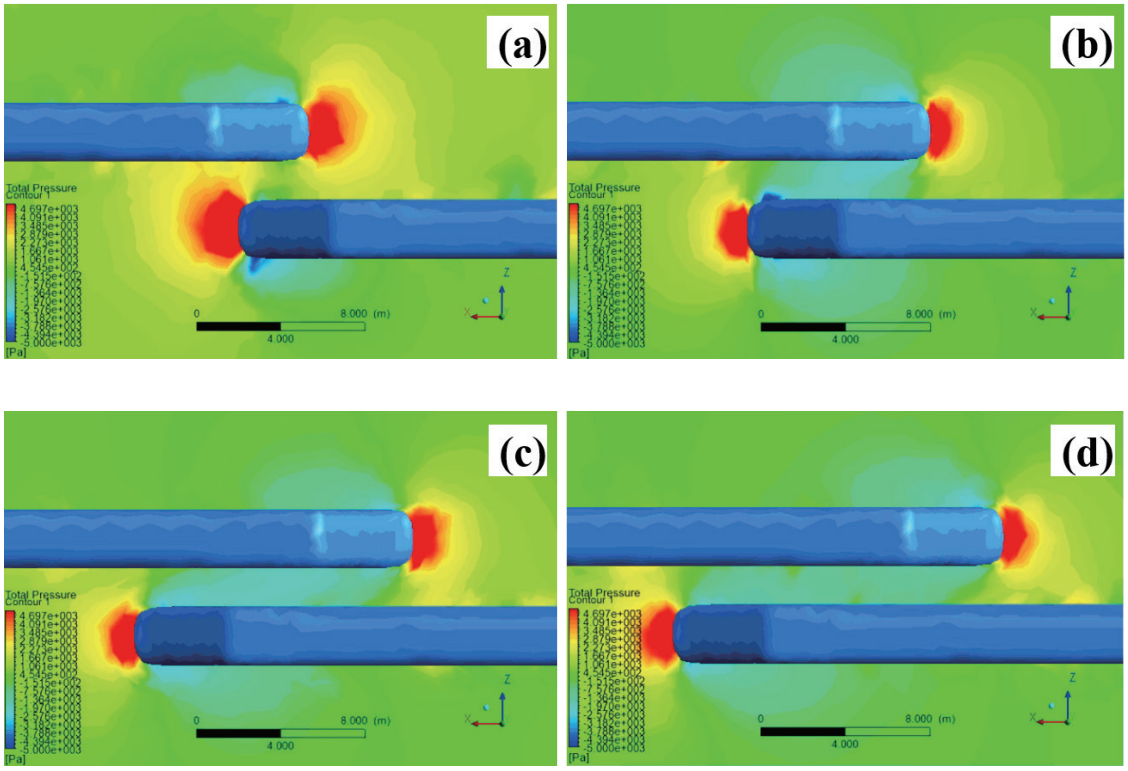

Fig. 4. (Color online) (a) At 3.0 s, the maximum positive pressure occurs. (b) At 3.05 s, the pressure sharply drops, reaching the maximum negative pressure. (c) By 3.15 s, the negative pressure between the two train bodies begins to increase. (d) At 3.2 s, negative pressure still exists between the train bodies, remaining at approximately −600 Pa.

pressure between the two train bodies remains negative but gradually increases, as shown in Fig. 4(c). At 3.2 s, the pressure between the train bodies stabilizes at approximately 600 Pa negative pressure, as shown in Fig. 4(d). The approach for selecting the pressure evaluation points in our simulation is based on the sensor placement reported in the referenced studies, spanning from the front of the train body to the nose section. From the data, it can be observed that the FEA simulation results of the high-speed train passing event align with the experimental data obtained from the sensors during the actual event. After comparing the results from our simulation with those in Refs. 9 and 19, the pressure data obtained from the experimental pressure sensors and the simulation results are judged to be similar, as shown in Table 1. The error between the maximum and minimum pressures of the experimental and simulation data is 16.89%. This error is relatively large and can be attributed to differences in the train design and the distance between the two trains. Despite this discrepancy, the overall trend, as seen in Fig. 5, mirrors the results in Refs. 9 and 10, confirming that the simulation data aligns with the experimental trends. Therefore, the validation results can be considered accurate. The results of this comparison highlights the reliability of the simulation model while also suggesting that certain factors, such as train design and relative positioning, can influence the results. Nonetheless, the general agreement between the experimental and simulated data provides confidence in the model's accuracy and its ability to predict pressure dynamics during high-

Table 1
Simulation results and data from Ref. 9.

	Pmax (Pa)	*Pmin* (Pa)	Δ*P* (Pa)	Error value
Data from Ref. 9 [R1]	1421	−1423	2844	16.89%
Simulation results	1700	−1600	3300	

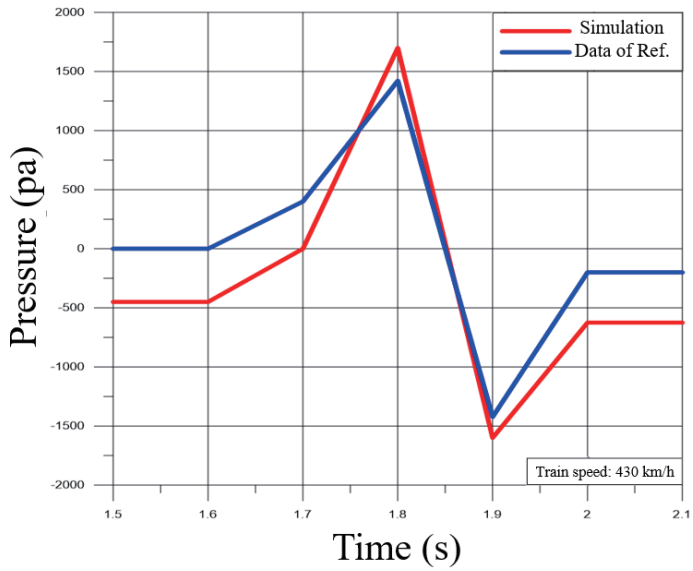

Fig. 5. (Color online) Simulation results and experimental data from Ref. 9.

speed train interactions. This validation process also emphasizes the importance of considering various external factors, such as train shape and spacing, when interpreting the simulation and experimental results of high-speed rail systems.

Since the two high-speed trains are operating in an open-air environment and the effects of crosswinds are not considered in this simulation, the airflow parameters at the moment of train passing are defined on the basis of the study by Niu *et al.*[11] In their study, the air density (ρ) was set to 1.225 kg/m^3 and the air viscosity (η) was set to 1.79×10^{-5} Pa·s. For the Reynolds number (*Re*) used in the simulation, when dealing with noncircular conduits—in this case, a rectangular cross section, as shown in Fig. 6(a), with height *a* and width *b*—the characteristic length (*L*) in the Reynolds number calculation is replaced by the hydraulic diameter (*Dh*). Since the simulated flow domain is rectangular, the hydraulic diameter is used instead of a typical diameter to represent the characteristic length.

$$Re = \frac{\rho V L}{\eta} \text{ and } L = Dh = \frac{4ab}{2(a+b)} = \frac{2ab}{a+b} \tag{1}$$

The calculation of the Reynolds number is essential in this study because it determines the flow regime and directly affects the selection of the turbulence model and meshing strategy used in the simulation. In high-speed train aerodynamics, the flow field surrounding the train body

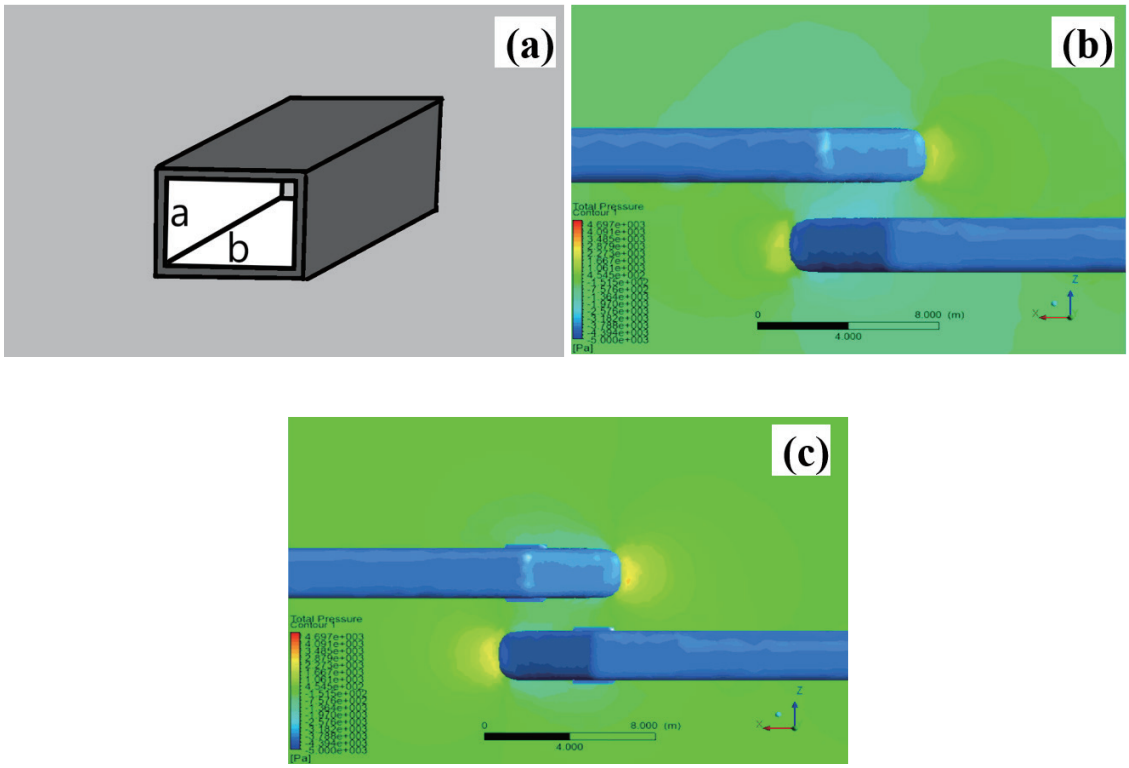

Fig. 6. (Color online) (a) Schematic diagram of the rectangular flow field, (b) negative pressure distribution of the train without stabilizing flow wings, and (c) negative pressure distribution of the train with stabilizing flow wings.

operates in a fully turbulent regime, and ensuring that the simulated Reynolds number matches that of actual high-speed operation is critical for reproducing realistic aerodynamic behavior. By computing the Reynolds number using the hydraulic diameter of the rectangular computational domain, the simulation properly reflects the physical conditions corresponding to the train speed, air density, and viscosity. This allows the numerical model to accurately capture the development of boundary layers, vortex structures, and pressure fluctuations during the train-passing event. Therefore, Eq. (1) is necessary because it establishes the fundamental flow characteristics of the simulation and ensures that the aerodynamic responses derived from the finite-element analysis correspond to the real-world Reynolds number conditions experienced by high-speed trains.

The simulation results reveal that during the moment two high-speed trains pass each other, a significant region of negative pressure and turbulent airflow is generated between the train bodies. This turbulence manifests as irregular vortex rings forming in the wake region, which not only disrupts the airflow but also reduces aerodynamic efficiency by increasing drag and diminishing the slipstream effect.[8] As a result, the overall train velocity experiences a slight reduction, highlighting a critical aerodynamic challenge in high-speed rail systems. At the precise moment of passing, the dramatic pressure differential between the two trains causes a mutual suction and subsequent repulsion effect. While such interactions have minimal impact on low-speed rail vehicles, in high-speed scenarios, these turbulent effects are significantly

amplified. The increased velocity enhances the dynamic interaction between the airflow and the train body, potentially affecting both stability and structural integrity. This type of turbulence is a well-documented phenomenon among high-speed vehicles. As they travel at elevated speeds, they must overcome the wall of air resistance in front of them.

Therefore, streamlining devices, such as stabilizing flow wings or aerodynamic fairings, are often implemented to guide airflow smoothly along the vehicle's surface and reduce aerodynamic drag.[12] In this study, we conducted a comparative simulation to evaluate the effectiveness of such devices. Specifically, we examined the moment of passing between two high-speed trains, both with and without stabilizing flow wings installed. As illustrated in Fig. 6(b), in the absence of these aerodynamic devices, the negative pressure generated between the trains is considerably higher. This is attributed to the intensified turbulence caused by the high-speed airflows clashing between the two moving bodies. In contrast, when stabilizing flow wings are present, the turbulent eddies are significantly reduced, as shown in Fig. 6(c). In this study, we conducted simulations across a range of stabilizing wing configurations, including different quantities (one to three pairs), geometric dimensions (widths from 0.3 to 0.6 m in 0.1 m increments and lengths from 1 to 4 m in 1 m increments), and installation positions along the train nose (from 2.0 to 4.4 m behind the foremost tip, in 0.8 m increments). Because the parameter space is extensive and the resulting flow interactions are highly complex, only the optimal configuration is presented and discussed in detail in this paper. The simulation results indicate that the best-performing configuration consists of a single pair of stabilizing flow wings installed 3.6 m behind the very front of the train. The optimal wing geometry is the lower-mounted stabilizing wing design with a width of 0.4 m and a length of 2 m.

In Fig. 7, the horizontal axis represents the interaction time between the two trains, while the vertical axis shows the corresponding pressure variation caused by turbulence as the trains

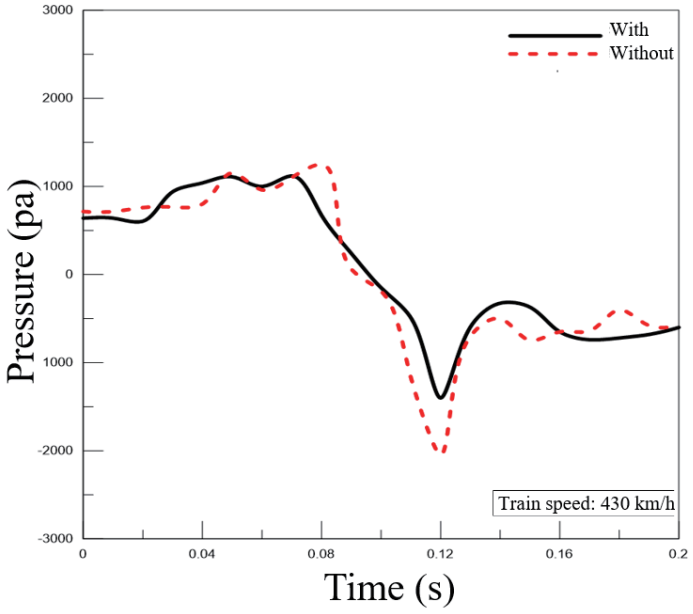

Fig. 7. (Color online) Differences in pressure variation caused by turbulence between the two trains with stabilizing flow wings and trains without stabilizing flow wings.

approach and pass each other. As illustrated in Fig. 7, the negative pressure generated in the space between the two trains is significantly reduced when stabilizing flow wings are installed. This reduction clearly demonstrates that the stabilizing wings effectively suppress the intensity of turbulence induced during the passing event. Compared with the configuration without stabilizing wings (maximum −2180 pa at 0.12 s), the proposed design improves the pressure-stabilizing performance by approximately 37% (−1373 pa at 0.12 s). Such a substantial improvement highlights the aerodynamic advantage of incorporating stabilizing wings into the train's nose-region design, contributing to enhanced operational stability and improved safety during high-speed train encounters.

4. Conclusions

In this study, we employed the Ansys Fluent module to establish a simulation methodology and conducted a literature review to validate the reliability of the simulation results. At a train speed of 430 km/h, the simulation showed that 2.9 s after the nose-to-nose alignment, the pressure at the simulation-based pressure evaluation locations on both train bodies gradually increased. At the 3 s mark, a peak positive pressure was observed, followed by a sudden drop to a negative pressure at 3.05 s. At 3.1 and 3.15 s, the negative pressure remained between the two train bodies, although the most intense negative pressure zone had already passed. This residual negative pressure continued to increase slightly, reaching approximately −600 Pa at 3.2 s during the body-to-body passing phase. When comparing the maximum and minimum pressure values obtained from this simulation to those measured by sensors in the referenced experimental studies, a deviation of 16.89% was observed. This relatively significant discrepancy is attributed to differences in train body design and the gap between the two trains during passing. Nonetheless, the overall pressure trend observed in the simulation closely matches the results reported in the referenced literature. Finally, we explored whether the addition of stabilizing flow wings to high-speed trains could lead to smoother pressure transitions during the passing event. The results indicate that, without stabilizing flow wings, significant turbulence occurs at the moment of train passing, potentially impacting operational safety. However, the addition of stabilizing flow wings was shown to effectively reduce pressure fluctuations between the two trains during their encounter.

Acknowledgments

This research was supported by Summit-Tech Resource Corp. and by projects under Nos. NSTC 113-2622-E-390-001 and NSTC 113-2221-E-390-011.

References

1 J. Niu, D. Zhou, F. Liu, and Y. Yuan: Tunnelling Underground Space Technol. **80** (2018) 139.
2 Z. Zhang and D. Z. Dan: J. Cent. South Univ. **44** (2013) 1672.
3 E. Deng, W. Yang, M. Lei, Z. Zhu, and P. Zhang: Eng. Struct. **188** (2019) 320.
4 M. Bocciolone, F. Cheli, R. Corradi, S. Muggiasca, and G. Tomasini: J. Wind Eng. Ind. Aerodyn. **96** (2008) 584.

5 X. H. He, Y. F. Zou, H. F. Wang Y. Han, and K. Shi: J. Wind Eng. Ind. Aerodyn. **135** (2014) 22.
6 B. Wu, S. Li, K. Li, Q. Yang, L. Zhang, and G. Qian: J. Wind Eng. Ind. Aerodyn. **196** (2020) 104050.
7 J. Muñoz-Paniagua and J. García: J. Wind Eng. Ind. Aerodyn. **184** (2019) 139.
8 J. R. Bell, D. Burton, M. Thompson, A. Herbst, and J. Sheridan: J. Wind Eng. Ind. Aerodyn. **134** (2014) 122.
9 S. Huang, Z. Li, and M. Yang: J. Wind Eng. Ind. Aerodyn. **188** (2019) 151.
10 D. Gao, F. Ni, G, Lin, S. Luo, and W. Ji: Energies **12** (2019) 3770.
11 J. Niu, D. Zhou, X. Liang, S. Liu, and T. Liu: J. Wind Eng. Ind. Aerodyn. **173** (2018) 187.
12 V. Shukla and A. K. Kaviti: Energy **126** (2017) 766.